Cite this paper: Vietnam J. Chem., **2021**, *59(5)*, 620-638 Research Article
DOI: 10.1002/vjch.202100016

Visible light photocatalytic degradation of organic dyes using W-modified TiO_2/SiO_2 catalyst

Nguyen Van Hung[1], Bui Thi Minh Nguyet[1], Nguyen Huu Nghi[1], Vo Thang Nguyen[2], Thai Vu Binh[3], Nguyen Thi Thanh Tu[4], Nguyen Nho Dung[5], Dinh Quang Khieu[6*]

[1]*Dong Thap University, 783 Pham Huu Lau, Cao Lanh City, Dong Thap 87000, Viet Nam*

[2]*University of Education and Science, The University of Danang, 459 Ton Duc Thang, Hoa Khanh Nam, Lien Chieu, Da Nang 55000, Viet Nam*

[3]*Insitute for Environment, Vietnam National University Ho Chi Minh city, 227 Nguyen Van Cu, District 5, Ho Chi Minh City 70000, Viet Nam*

[4]*Faculty of Technology, Van Lang University, 45 Nguyen Khac Nhu, Co Giang, District 1, Ho Chi Minh City, 70000, Viet Nam*

[5]*Danang Sport University, 44 Dung Si Thanh Khe, Thanh Khe Tay, Thanh Khe, Da Nang 55000, Viet Nam*

[6]*University of Sciences, Hue University, 77 Nguyen Hue, Phu Nhuan, Hue City, Thua Thien Hue 53000, Viet Nam*

Submitted March 3, 2021; Revised June 11&18, 2021; Accepted July 13, 2021

Abstract

In the present study, the synthesis of W-modified TiO_2/SiO_2 composite and its catalytic activity in the visible light region is demonstrated. The W-modified TiO_2/SiO_2 composite was obtained from the hydrolysis of a mixture containing titanium (IV) oxysulfate, ammonium metatungstate, and SiO_2 powder in an alkaline medium. The obtained materials were characterized by using X-ray diffraction (XRD), Fourier transformation-infrared spectroscopy (FT-IR), high-resolution transmission electron microscopy (HRTEM), energy dispersive X-ray elemental mapping observation, nitrogen adsorption/desorption isotherms, photoluminescence spectra (PL), and ultraviolet visible diffusive reflectance spectroscopy (UV-Vis DRS). In this material, W-modified TiO_2 nanoparticles of about 3-5 nm were highly dispersed on the silica network. Both W-modified TiO_2 and W-modified TiO_2 decorated on the SiO_2 substrate significantly promoted the visible light absorption of the material. The photocatalytic activity of the prepared catalyst was assessed through the photodegradation of Methylene blue, Rhodamine-B, Methyl orange, and Congo red dyes under visible light illumination. It was found that the kinetic and equilibrium data of the photocatalytic process fitted the modified Langmuir-Hinshelwood model well. Recyclable studies have shown that the catalyst still retained its original activity after the third cycle.

Keywords. W-modified TiO_2, silica, organic dyes, photocatalytic degradation.

1. INTRODUCTION

The synthetic dyes have been widely used in various industrial fields such as dyeing, textiles and plastics. It is estimated that about 100.000 dyes are commercially available with more than 7×10^5 tones of dyes produced annually.[1] In industry, most of synthetic dyes employed currently belong to the azo group such as Methylene blue (MB), Rhodamine-B (RhB), Methyl orange (MO), Congo red (CR) due to their high stability in washing process and in the natural condition. Even small amount of dyes (a few ppm) in aquatic resources is undesirable because of the presence of non-biodegradable toxic colour pigments which can be dangerous and carcinogentic that harm greatly to human beings and aquatic species.[1,2] Therfore, the elimination of organic dyes in waste waters has been critical and compulsory. Techniques such as adsorption[3], coagulation[4], and electrochemistry[5] are widely available for removing organic dye contaminants. However, these processes generate secondary pollutions which require additional treatment steps. Recently, the photocatalytic degradation method has been considered as a promising alternative approach in waste water treatment.[6,7]

Among many semiconductors with photocatalytic activity such as TiO_2, WO_3, $SrTiO_3$, Fe_2O_3, ZnO, ZnS and CdS. TiO_2 has been proved to be the most suitable one for applications in environmental treatment because of its excellent photocatalytic activity under suitable condition, inert chemistry and biology, sustainability and low cost.[7,8] However, because of large bandgap energy (about 3.2 eV), pristine TiO_2 can only exhibit photocatalytic activity when irradiated by ultraviolet light which limits the ability to take advantage of the abundant light energy from the solar light.[9] Various techniques such as doping with major subgroup metals[10,11] or transition metals,[12,13] nonmetals,[9,14] and combining with other semiconductors[15] have been employed to reduce the optical band gap energy and further expand the scope of application of TiO_2. Among transition metals that can be used as dopants, tungsten is considered to be able to prevent the recombination of excited electron-hole pairs, narrow bandgap energy and increase acidity on the surface of the catalyst, resulting in improving photocatalytic activity of TiO_2 in the visible light area.[15-17] Although photocatalysts in the fine powder form often show better photocatalytic activity, using fine powder catalysts might lead to some disadvantages such as the difficulty in separating and recycling them and especially a feasible agglomeration resulting in a significant reduction of catalytic activity. Employing different substrates such as carbon,[18] silica,[19-21] rectorate,[22] and montmorillonite clay[23] can provide a potential solution to these problems. Among these substrates, SiO_2 is often more preferred, because not only it can improve the surface area of composite materials, it can also penetrate into the TiO_2 crystal lattice structure (due to the smaller ion radius of Si^{4+} ion compared to Ti^{4+}, 0.041 nm compared to 0.064 nm), creating beneficial defects, thereby enhancing the photocatalytic efficiency in visible light for TiO_2.[24]

Recently, TiO_2/SiO_2 doped by transition metal ions materials have gained much attention thanks to outstanding advantages such as particularly large specific surface area, high surface acidity, abundant surface hydroxyl groups, low recombination of photo induced electrons/holes pair which can enhance the photocatalytic activity efficiency. Liu *et al.*[19] reported that 0.2 % of Ce-doped SiO_2/TiO_2 fibers exhibited higher photocatalytic activity toward decomposition of MB than Degussa P25 and the samples doped with only Ce or SiO_2 did. Recently Chen *et al.*[25] reported that graphene oxide/WO_3 quantum dots/TiO_2@SiO_2 possessed excellent photocatalytic performance under UV light or solar light.

In the present paper, we report the loading of W-modified TiO_2 nanoparticles onto the SiO_2 substrate through hydrolysis of titanium (IV) oxysulfate, ammonium metatungstate, and SiO_2 powder in alkaline environment. The purpose of the study is to evaluate photocatalytic activity of W-modified TiO_2/SiO_2 composite through the ability to decompose Methylene blue, Rhodamine-B, Methyl orange and Congo red dyes in aqueous solution under visible light irradiation. Kinetics analysis on dyes decomposition by W-modified TiO_2/SiO_2 material was also addressed.

2. MATERIALS AND METHODS

2.1. Materials

The source of SiO_2 material was received from the Center of Chemical Analysis, Dong Thap University with characteristic phase structure (according to XRD spectrum), specific surface area (according to BET (S_{BET}) analysis), and composition of elements (by using EDX) summarized in table 1.

Table 1: Physical chemical properties of SiO_2

Material SiO_2	XRD	S_{BET} ($m^2.g^{-1}$)	EDX (wt. %)		
			Si	O	Other
	Amorphous	383.8	42.66	56.44	0.90

Sodium hydroxide (NaOH, ≥ 99 %), hydrochloric acid (HCl, 37 %), potassium iodide (KI, ≥ 99.5 %), isopropanol ($CH_3CH(OH)CH_3$, IPA, ≥ 99.8 %), sodium chloride (NaCl, ≥ 99.5 %) were purchased from Merck. Titanium (IV) oxysulfate ($O_5STi.xH_2O$, ≥ 29 % (as TiO_2 basis)), ammonium metatungstate ($H_{26}N_6O_{40}W_{12}.xH_2O$, ≥ 99.0 % WO_3 basis) methylene blue ($C_{16}H_{18}N_3SCl.xH_2O$, 99.5 %), Rhodamine-B ($C_{28}H_{30}N_2O_3$, ≥ 96.5 %), Methyl orange ($C_{14}H_{14}N_3NaO_3S$, Dye content, 85 %), Congo red ($C_{32}H_{22}N_6Na_2O_6S_2$, ≥ 97 %), 1,4- benzoquinone ($C_6H_4O_2$, BQ, ≥ 99 %) and dimethyl sulfoxide ($(CH_3)_2SO$, DMSO, 99.9 %) were obtained from Sigma - Aldrich. All used chemicals were of analytical grade and were used as received without any further purification. Table 2 shows the physicochemical properties and structure of the Methylene blue (MB), Rhodamine-B (RhB), Methyl orange (MO), and Congo red (CR).[2,3,26,27]

2.2. Methods

2.2.1. Synthesis of W-modified TiO_2/SiO_2

In a typical synthesis, 4.0 g of titanium(IV) oxysulfate (0.025 mol) and 123.2 mg of ammonium metatungstate ($0.5.10^{-3}$ mol, W/Ti molar ratio of 0.02) were dissolved in 110 mL of distilled water and stirred variously for 30 minutes at room temperature. Then, 1.0 g of SiO_2 and 40 mL of 1 M NaOH were added into this solution under stirring for about 6 hours. The obtained solid was separated by centrifugation and washed several times with distilled water until the filtrate was neutral. It was then dried at 105 °C for 24 hours. The final solid was heated at 600 °C for 2 hours with a ramping rate of 10 °C/min to obtain W-modified TiO_2/SiO_2. TiO_2 and TiO_2/SiO_2 samples were also prepared in the same manner but in the absence of ammonium metatungstate/SiO_2 and ammonium metatungstate, respectively.

Table 2: Some physicochemical properties and structure of dyes (M_W means molecular weight and λ_{max} means maximum absorption wavelength)

Dyes	Molecular structure	Molecular size (nm) [26, 28]	M_W (g.mol^{-1})	λ_{max} (nm)	pK$_a$
MB	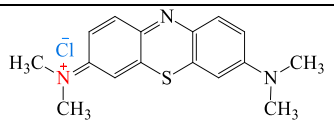	1.26×0.77×0.65	319.85	665	3.8
RhB	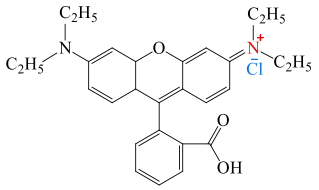	1.59×1.18×0.56	479.02	554	3.7
MO	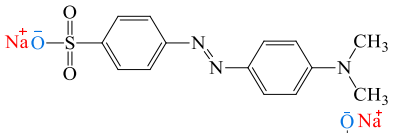	1.31×0.55×0.18	327.33	465	3.4
CR	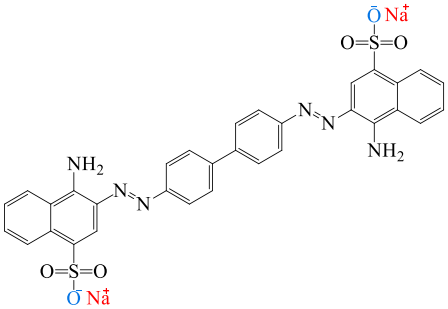	2.62×0.74×0.43	696.67	497	5.5

2.2.2. Characterization of materials

X-ray diffraction (XRD) was performed by a MiniFlex 600 diffractometer (Rigaku, Japan) with the radiation source, CuKα, $\lambda = 0.15406$ nm. The scanned angle (2θ values) range was between 10 and 80° with a step size of 0.01°. The transmission electron microscopy (TEM) and high-resolution transmission electron microscopy (HRTEM) was performed using a JEOL JEM-1400 (USA) and JEOL JEM-2100 (USA), respectively to characterize the morphologies of the samples. Elemental mapping observation and composition of elements were determined by means of electron dispersive X-ray (EDX) analysis coupled with HRTEM using a JEOL 2100, EDX detector with XMax 80 T (Oxford). Fourier Transformation-Infrared (FT-IR) spectra of the samples were recorded on an IR Affinity-1S spectrophotometer (Shimadzu). UV-Vis-DRS spectra were recorded with the UV-2600 (Shimadzu) instrument. The nitrogen adsorption/desorption isotherms were determined by using a Quantachrome TriStar 3000 V6.07A adsorption instrument. The photoluminescence spectra (PL) were measured by using a Horiba Fluorolog 3 FL3-22 with the excitation light at 370 nm.

2.2.3. Photocatalytic activity experiments

In this work, a beaker containing 500 mL of each dye (30 to 70 mg.L^{-1}) and 300 mg of catalyst was placed under a lamp bracket. The light source was a 45 W - 220 V Compact lamps (Dien Quang) equipped with a wavelength cut-off filter ($\lambda \leq 420$ nm, d = 77 mm). Prior to illumination, the suspension was stirred magnetically in the dark for 60 min to establish adsorption/desorption equilibrium. Three milliliters of the suspension were withdrawn at a certain interval

time and and then centrifuged to remove the solid catalyst. The concentration of dyes in the supernatant was determined by UV-Vis spectrophotometry (Spectro UV-2650, Labomed - USA) at maximum wavelengths of 664, 552, 464, and 498 nm for MB, RhB, MO, and CR, respectively. The adsorption efficiency of dye (A%) was calculated from:

$$A(\%) = 100 \times (C_0 - C_t)/C_0 \quad (1)$$

where C_0 (mg.L^{-1}) is the initial concentration of dye and C_t (mg.L^{-1}) is the concentration of dye at adsorption time t (min).

The photodegradation efficiency of the photocatalyst was calculated according to expression:

$$D(\%) = 100 \times (C_{0e} - C_t)/C_{0e} \quad (2)$$

where C_{0e} (mg.L^{-1}) and C_t (mg.L^{-1}) are the dye concentration at sorption equilibrium time and at irradiated time of t (min), respectively.

The dye decolorization performance was calculated using the formula (Eq. 3):

$$E(\%) = 100 \times (C_0 - C_f)/C_0 \quad (3)$$

where C_0 (mg.L^{-1}) and C_f (mg.L^{-1}) are the initial and final concentration of the dye solution, respectively.

Total organic carbon (TOC) of the initial and irradiated samples was determined using a TOC analyzer (Model: Aurora 1030C TOC Analyzer, OI Analytical - USA). TOC removal efficiency was calculated by following equation (4):

$$R(\%) = 100 \times (TOC_{0e} - TOC_t)/TOC_{0e} \quad (4)$$

where TOC_{0e} and TOC_t are the TOC values at sorption equilibrium time and at irradiated time of t (min), respectively.

To investigate the pH effect, 300 mg of W-modified TiO_2/SiO_2 were added to the beakers containing 500 mL of 40 mg/g MB, RhB, MO and CR, respectively. The pH of the solution was adjusted to a desired value (in the range of 3-11) by using 0.1 M NaOH or 0.1 M HCl. The suspension of catalyst and dye was first stirred for 60 minutes in the dark to ensure adsorption/desorption equilibrium and then illuminated by the visible-light for 120 minutes. The dye concentration in the liquid after being separated from the solid by centrifugation was determined by photo-spectroscopy. The leaching test was also conducted in a similar manner where the catalyst was filtered out after 30 minutes ofillumination and the suspention or solution were taken out to determine dye concentration. Leaching experiments were performed at pH of 3 for MO and CR solutions and pH of 9 for MB and RhB. The blank experiment without the catalyst was also performed to test the photolysis of dyes.

In the free radical scavenging test, KI; BQ; DMSO and IPA were used as scavengers. A suspension of 500 mL of each dye (40 mg.L^{-1}) and 300 mg catalyst was first stirred for 60 min in the dark before 20 mL of 2.4×10^{-2} M each radical scavenger was introduced into the mixture simultaneously with visible-light illumination. The concentrations of MB, RhB, MO, and CR dyes were determined by UV-Vis spectrophotometry as stated above.

3. RESULTS AND DISCUSSION

3.1. Characterization

Figure 1 presents the XRD patterns of TiO_2, SiO_2, TiO_2/SiO_2 and W-modified TiO_2/SiO_2 samples. As observed in Figure 1, the SiO_2 sample exhibits low intensity and broad diffraction peak at 2 theta angle of about 22.3°, which is typical for the amorphous structure of SiO_2.[29] TiO_2 sample exhibits diffraction with high intensity at the angle 2θ = 25.22° corresponding to (1 0 1) plane of anatase phase (JCPDS-00-001-0562). XRD patterns of TiO_2/SiO_2 and W-modified TiO_2/SiO_2 also show the characteristic diffraction for TiO_2 anatase but with lower diffraction intensity and broader nature. These peaks also shift to smaller 2-theta angle than that of the original TiO_2 pattern indicating that there is a deformation of TiO_2 lattice which may be due to the formation of new Ti-O-Si bond instead of Ti-O.[24,30] It is interesting that in the XRD pattern of W-modified TiO_2/SiO_2 material, except characteristic anatase phase of TiO_2 at 2θ = 25.22°, not any peaks of the WO_3 phase or any other strange phase can be detected, which could be due to the participation of W^{6+} ions in the aggregation of TiO_2 crystal lattice structure.[24,31] The particle size of TiO_2 crystal in TiO_2; TiO_2/SiO_2 and W-modified TiO_2/SiO_2 materials calculated according to Scherrer equation based on diffraction peak (1 0 1) is 7.1 nm; 3.7 nm and 4.0 nm, respectively. The suppression of TiO_2 crystal growth in SiO_2 structure could lead to a decrease in particle size of TiO_2 in TiO_2/SiO_2 and W-modified TiO_2/SiO_2 samples.

The presence of different functional groups on the obtained samples was confirmed by FT-IR (figure 2). In four samples, the band at 3000-3600 cm^{-1} is assigned for O-H (free) and O-H (H-bonded) vibrations.[24,30,31] The peak at 2360 cm^{-1} is due to the absorption of CO_2 molecules on the sample surface[32,33] during sample storage. FT-IR spectrum of SiO_2 shows the absorption peaks at 467.8 and 805.3 cm^{-1} corresponding to the stretching vibration of the Si–O bond and the absorption peaks at 960.6

and 1094.6 cm^{-1} of the stretching vibration of Si–OH and Si–O–Si bonds, respectively.[30] Meanwhile, the IR spectrum of the TiO_2 sample exhibits an absorption peak at 460.0 cm^{-1} which can be assigned to the vibration of Ti–O–Ti bond.[24,30] The vibrations of Si–O and Si–OH peaks in TiO_2/SiO_2 and W-modified TiO_2/SiO_2 samples reduce in intensity and shift to higher energy compared to the pristine SiO_2 sample, probably due to Ti–O–Si bond formation in TiO_2/SiO_2 and W-modified TiO_2/SiO_2 materials.[24,30,31]

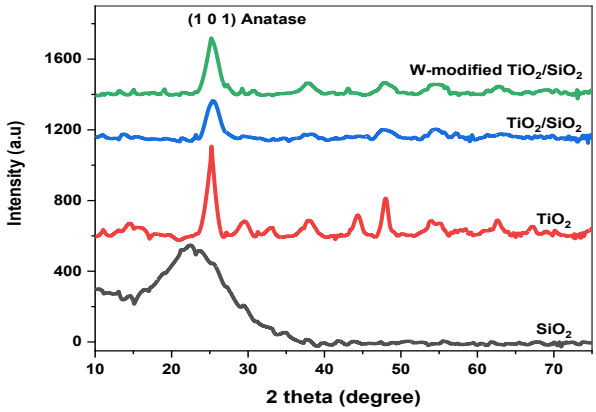

Figure 1: XRD patterns of the TiO_2, SiO_2, TiO_2/SiO_2, and W-modified TiO_2/SiO_2 samples

The morphology of the obtained materials was examined by TEM and HRTEM images (figure 3). It can be seen that TiO_2 is in the form of crystalline nanoparticles with an average size of about 7-10 nm (figure 3a) while SiO_2 samples exist as spherical particles with diameters ranging from 100-200 nm (figure 3b). The TiO_2 and W-modified TiO_2 particles seem to be embedded in the SiO_2 matrix (Fig. 3c and Fig. 3d, respectively), where the particle size of TiO_2 (about 3-5 nm) is smaller than that of primary TiO_2 (about 7-10 nm), which is consistent with the XRD spectrum analysis. The HR-TEM image of the W-modified TiO_2/SiO_2 sample (figure 3e) shows the lattice fingers with interplanar distances of 0.35 and 0.24 nm, corresponding to the (1 0 1) and (1 0 3) planes of anatase phase.[16,34]

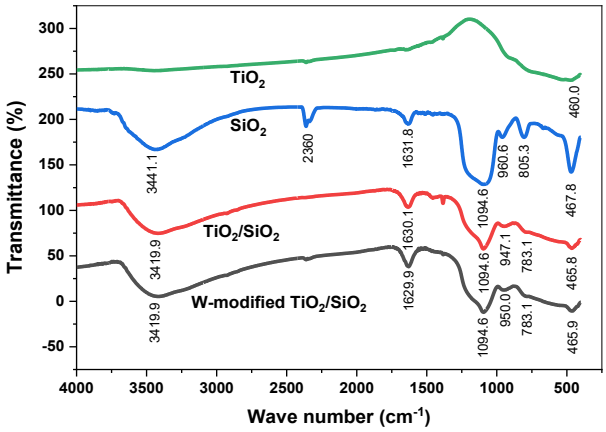

Figure 2: FT-IR spectra of TiO_2, SiO_2, TiO_2/SiO_2, and W-modified TiO_2/SiO_2 samples

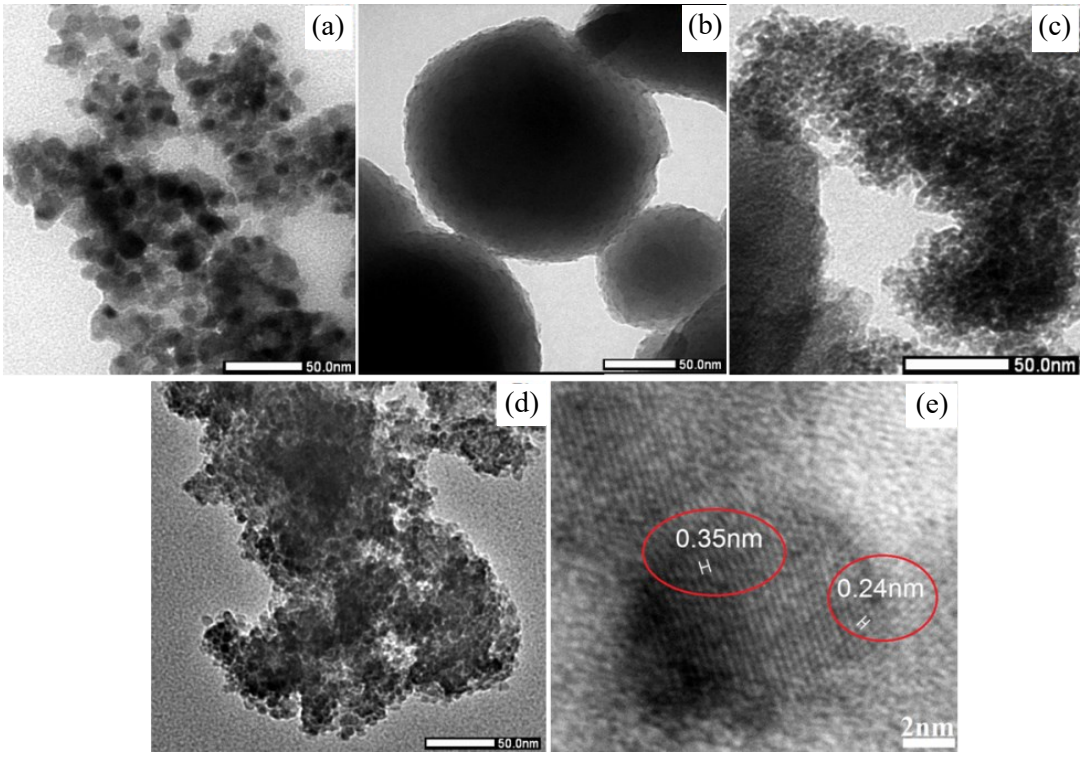

Figure 3: TEM observation of (a) TiO_2, (b) SiO_2, (c) TiO_2/SiO_2, and (d) W-modified TiO_2/SiO_2, (e) HR-TEM image of W-modified TiO_2/SiO_2 composite

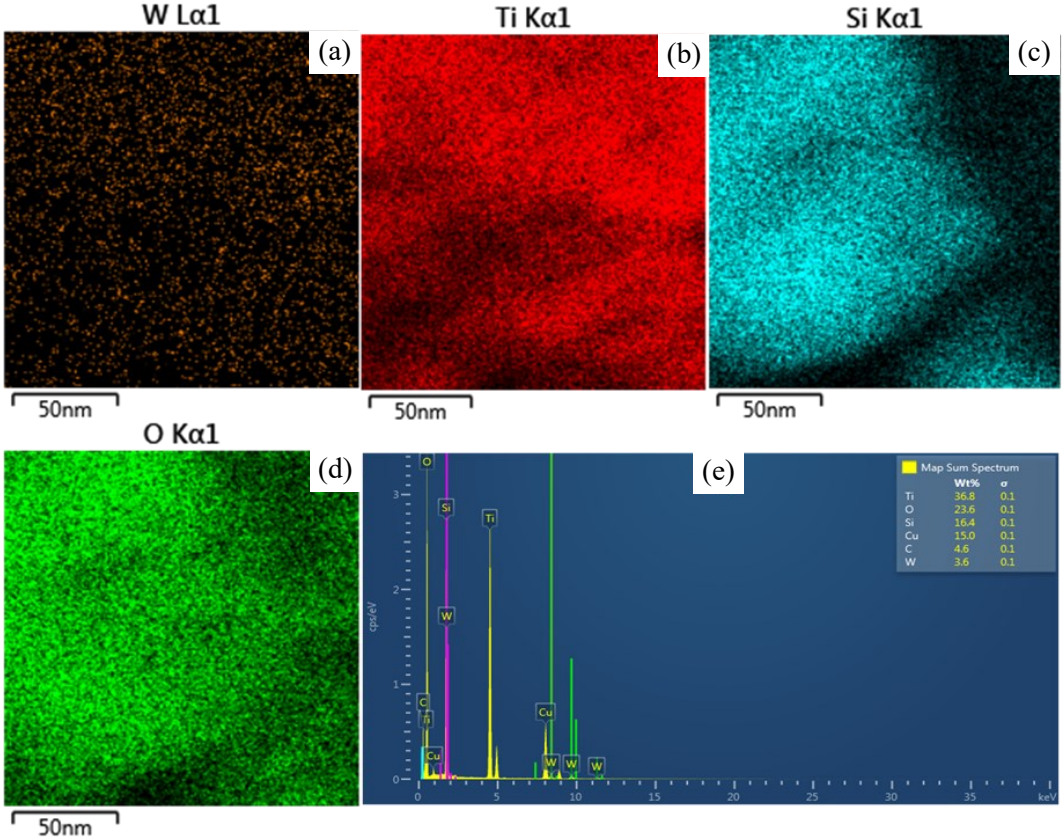

Figure 4: Corresponding element mapping of (a) tungsten, (b) titanium, (c) silicon, and (d) oxygen; (e) EDX spectrum of W-modified TiO_2/SiO_2 composite

The EDX-elemental mapping of a selected area in the W-modified TiO_2/SiO_2 sample is shown in figure 4. The existence of W (figure 4a), Ti (figure 4b), Si (figure 4c) and O (figure 4d) confirm the spatial distribution of elements on structures of W-modified TiO_2/SiO_2 composite. EDX analysis further verified the presence of W, Ti, Si and O components in W-modified TiO_2/SiO_2 (figure 4e). The surface composition was found to be W 3.6 %; Ti 36.8 %; Si 16.4 %; O 23.6 %; C 4.6 % and Cu 15.0 % (figure 4e, inset). The presence of C and Cu signal comes from the C/Cu substrate of the measurement. These results demonstrate that the W-modified TiO_2 nanoparticles have been successfully dispersed on the SiO_2 substrate and confirm a high purity of the synthesized W-modified TiO_2/SiO_2 material.

The adsorption properties of the obtained samples were investigated using the nitrogen adsorption-desorption isotherms at 77 K (figure 5). The isothermal curve of TiO_2 belongs to type IV with hysteresis loop H1 according to the classification of IUPAC, implying a mesoporous structure of the material.[35] Whereas all three samples of SiO_2, TiO_2/SiO_2 and W-modified TiO_2/SiO_2 possess isothermal curves of type IV with hysteresis loop H3, which is characteristic for materials that exist simultaneously in two forms of microporous and mesoporous structures.[36,37] The specific surface area of the composite samples, derived from the isotherm, decreases in the order of SiO_2 (383.8 $m^2.g^{-1}$) > TiO_2/SiO_2 (321.4 $m^2.g^{-1}$) > W-modified TiO_2/SiO_2 (319.1 $m^2.g^{-1}$) > TiO_2 (99.5 $m^2.g^{-1}$). The results indicate that the formation of the W-modified TiO_2/SiO_2 composite significantly enhanced the specific surface area of the TiO_2 precursor.

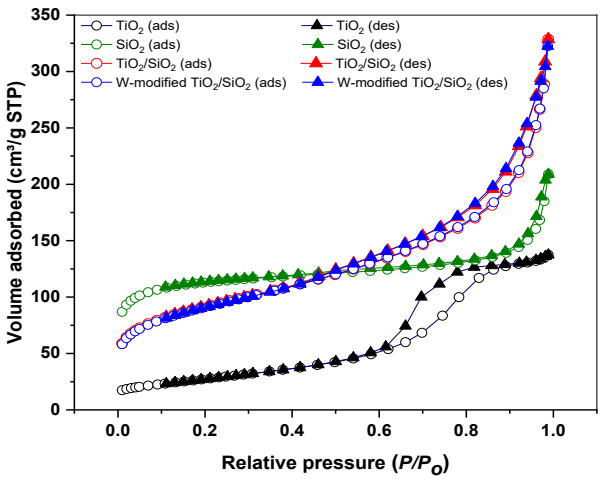

Figure 5: Nitrogen adsorption-desorption isotherms of TiO_2, SiO_2, TiO_2/SiO_2, and W-modified TiO_2/SiO_2 samples

UV-Vis DRS spectra of TiO_2, SiO_2, TiO_2/SiO_2 and W-modified TiO_2/SiO_2 samples are shown in figure 6. It was found that the SiO_2 sample has no optical absorption within the entire measured wavelength range, while the pristine TiO_2 sample absorbs light in the wavelength of 250-400 nm. The cooperation of TiO_2 into TiO_2/SiO_2 and W-modified TiO_2/SiO_2 composite has enhanced the visible-light absorption of TiO_2, evidenced by a redshift to the visible light region. The direct bandgap energy of TiO_2 (3.01 eV), TiO_2/SiO_2 (2.97 eV) and W-modified TiO_2/SiO_2 (2.85 eV) was calculated by Tauc's plot (figure 6b).

PL emission is associated with the formation of photochemical charged particles and their recombination kinetics. Therefore, PL spectra were used to study the existence of photo-electron-hole pairs in a photocatalyst. Figure 7 shows the PL spectra of TiO_2, SiO_2, TiO_2/SiO_2, and W-modified TiO_2 /SiO_2. In all four samples, the emission area ranges from 400-550 nm with different PL intensities. The addition of SiO_2 or W^{6+} ion doping can slow down the recombination of photoinduced electrons/holes pairs in TiO_2. Indeed, the PL intensity of the W-modified TiO_2/SiO_2 sample was the lowest compared to the bare TiO_2, SiO_2, and TiO_2/SiO_2, suggesting that the recombination of photoinduced electrons/holes in this material was effectively prevented.[38] The extended lifetime of charged particles can, in turn, promote the photocatalytic activity of W-modified TiO_2/SiO_2 composite.

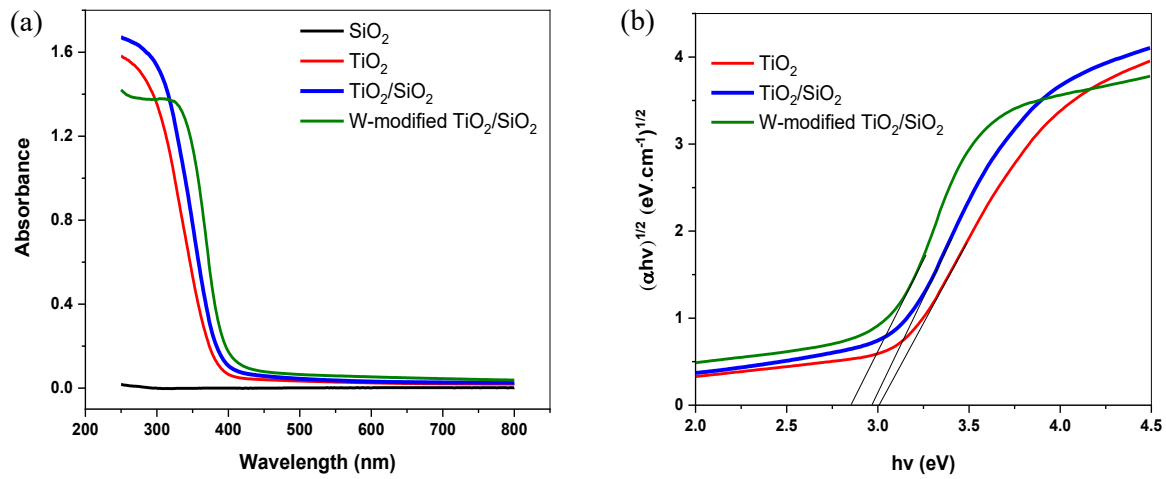

Figure 6: (a) DRS-UV-Vis spectra of TiO_2, SiO_2, TiO_2/SiO_2, and W-modified TiO_2/SiO_2; (b) Tauc's plots for TiO_2, TiO_2/SiO_2, and W-modified TiO_2/SiO_2

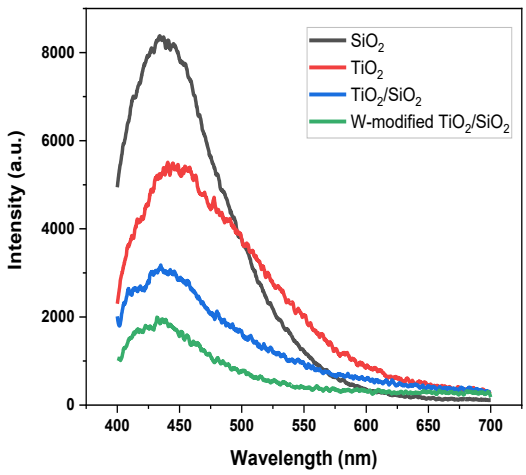

Figure 7: Photoluminescence (PL) spectra of TiO_2, SiO_2, TiO_2/SiO_2, and W-modified TiO_2/SiO_2

3.2. Visible light-driven photocatalytic degradation of dyes

3.2.1. Photodegradation of dyes with different catalysts

Figure 8 shows the adsorption and photodegradation efficiency of MB, RhB, MO, and CR dyes using the TiO_2, SiO_2, TiO_2/SiO_2, and W-modified TiO_2/SiO_2 catalysts. The SiO_2 sample has the highest MB, RhB, MO and CR dyes adsorption efficiency, followed by W-modified TiO_2/SiO_2 and TiO_2/SiO_2 and the lowest was primary TiO_2 (figure 8). Although the SiO_2 sample possesses the highest adsorption capacity, it exhibits the lowest photocatalytic efficiency for MB, RhB, MO and CR (7.71 %, 6.48 %, 5.49 % and 3.95 %, respectively), followed by TiO_2 (11.08 %, 9.39 %, 7.82 % and 5.68 %) and TiO_2/SiO_2 (33.20 %, 28.83 %, 24.27 % and 17.13 %). W-modified TiO_2/SiO_2 shows the highest degradation efficiency of 99.67, 83.61, 70.39 and 50.52 % for MB, RhB, MO and CR, respectively. The results are in good agreements with the narrowing of the bandgap energy

with the order of TiO_2 (3.01 eV) > TiO_2/SiO_2 (2.97 eV) > W-modified TiO_2/SiO_2 (2.85 eV) (figure 6) as well as the decrease in the intensity of PL emission in the order from SiO_2 to W-modified TiO_2/SiO_2 (Figure 7). These results indicate that the photocatalytic activity of TiO_2 in W-modified TiO_2/SiO_2 is significantly enhanced in the visible light region.

(a)

3.2.2. Effect of pH and leaching experiment

The pH of the solution can decide the charge on the catalyst surface, which affects the dye removal performance. Effects of pH of solution on the decolorization performance of W-modified TiO_2/SiO_2 on two different categories of dyes: MB and RhB - cationic dyes; MO and CR - anionic dyes are shown in figures 9a and 9b, respectively.

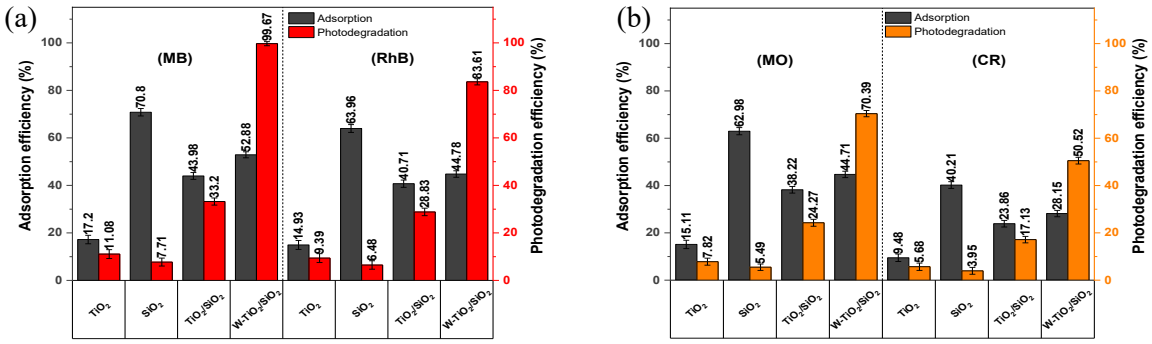

Figure 8: The adsorption and photodegradation efficiency of (a) MB, RhB and (b) MO, CR dyes over TiO_2, SiO_2, TiO_2/SiO_2 and W-modified TiO_2/SiO_2 catalysts (V = 500 mL, C_0 = 40 mg.L^{-1}; $m_{catalyst}$ = 300 mg; pH = 9 for MB, RhB and pH = 3 for MO, CR; adsorption time = 60 min. and illumination time = 120 min.)

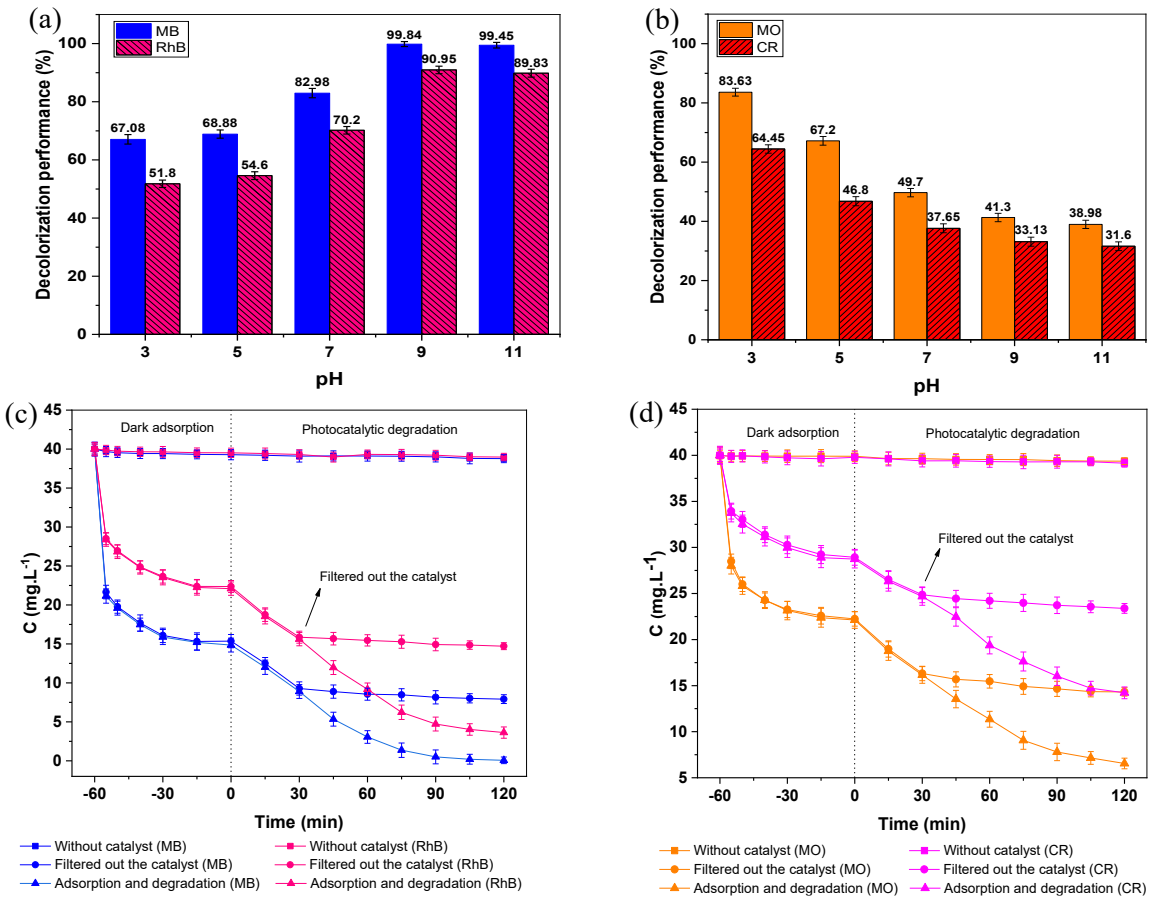

Figure 9: Effect of pH on decolorization performance of (a) MB, RhB and (b) MO, CR dyes over W-modified TiO_2/SiO_2 catalyst; leaching experiments for (c) MB, RhB and (d) MO, CR (V = 500 mL, C_0 = 40 mg.L^{-1}; $m_{catalyst}$ = 300 mg; adsorption time = 60 min.; illumination time = 120 min)

Figure 9a shows that the decolorization performance of MB and RhB is the lowest at pH of 3 and rises slightly at pH of 5. However, at pH ≥ 7, it increases significantly and reaches the highest one of 99.84 and 90.95 %, respectively, at pH 9. Meanwhile, figure 9b illustrates that the decolorization performance of MO and CR in the presence of W-modified TiO_2/SiO_2 catalyst decreases from 83.63 % and 64.45 % to 38.98 % and 31.60 %, respectively, upon increasing pH value of the solution from 3 to 11. As pH increases, the catalyst surface become less postively charged and resulted in an increase in electrostatic intraction with cationic-dyes enhancing dye adsorption capacity, accordingly photocatalytic degradation. The opposite is true for the anionic dyes in which increasing repulsive interaction resulted in decreasing adsorption capacity as well as dropping photocatalytic degradation as pH increases. In general, the results show that W-modified TiO_2/SiO_2 materials are capable for photocatalytic decomposing of variety of dyes in solution.

The kinetics of the decolorization of MB, RhB, MO and CR dyes and the leaching test are shown in Figures 9c and 9d. The decolorization of those dyes was not observed if visible light was irradiated in the absence of W-modified TiO_2/SiO_2 suggesting that they were stable and did not undergo photolysis. In the leaching experiment, the catalyst was filtered after 30 minutes of irradiation. It was found that the colors of the solutions were almost unchangeable as the resulting solution was continued to irradiate for further 90 minutes. Therefore, it can be inferred that W-modified TiO_2/SiO_2 acts as a heterogeneous catalyst in nature.

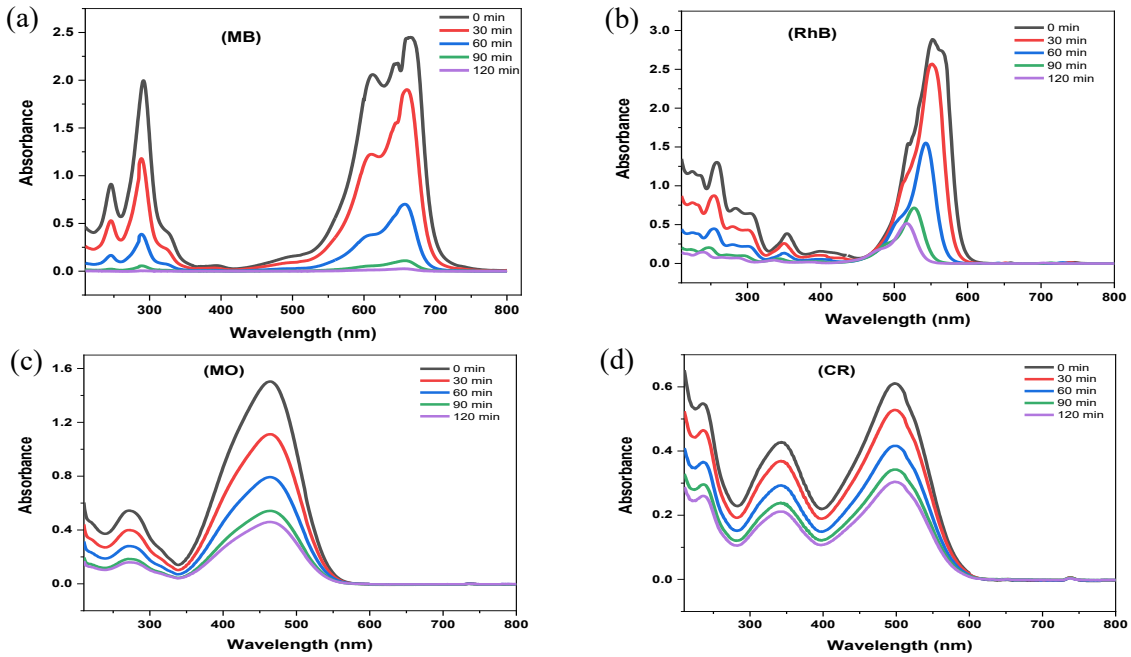

Figure 10: UV-Vis absorption spectra of solutions for (a) MB, (b) RhB, (c) MO, and (d) CR dyes at different illumination times (V = 500 mL; C_0 = 40 mg.L^{-1}; $m_{catalyst}$ = 300 mg; pH = 9 for MB and RhB and pH = 3 for MO and CR; adsorption time = 60 min. and illumination time from 0 to 120 min.)

3.2.3. Visible-light-driven photocatalytic degradation of dyes

Figure 10 shows the UV-Vis spectra of solutions of MB, RhB, MO and CR dyes at different decomposition times. It can be seen that the spectrum of each dye solution was characterized by two major absorption regions; one is in the ultraviolet region (292, 258, 272 and 344 nm, respectively) and another is recorded in the visible region (664, 552, 464 and 498 nm, respectively).

The ultraviolet absorption regions refers to $\pi \rightarrow \pi^*$ electron transfer of the aromatic rings in the dye molecules, whereas the absorbance at the visible region are attributed to $n \rightarrow \pi^*$ electron transfer in the azoic groups.[39-41] Generally, the absorption intensity of the peaks of the dyes gradually decreases upon extending lighting time without detection of any new peaks. This implies that the dyes are continuously degraded during the photocatalytic processes through the chromophore destruction.[39,42]

The TOC test is also used to examine the MB, RhB, MO and CR dyes mineralization during photocatalytic decomposition (Figure 11). With initial equal concentrations of 40 mg.L^{-1} MB, RhB, MO and RhB dyes, after 60 minutes of dark

adsorption, the equilibrium concentration of the dyes was determined as 18.85 mg.L^{-1}, 22.09 mg.L^{-1}, 22.12 mg.L^{-1} and 28.74 mg.L^{-1} which correspond to TOC_{0e} values of 11.97 mg.L^{-1}, 17.76 mg.L^{-1}, 10.18 mg.L^{-1}and 502.95 mg.L^{-1}. After 120 minutes of illumination, final TOC values of MB, RhB, MO and CR dyes were 0.04, 3.45, 3.01 and 248.85 mg.L^{-1}, respectively. Figure 11 shows that MB is almost completely mineralized with a TOC removal efficiency of 97.12 %, followed by RhB (80.59 %), MO (67.84 %) and CR (46.51 %).

It is well known that photocatalytic decomposition is related to the oxidation of organic molecules by active radicals (hydroxyl $^{\bullet}OH$ radicals, superoxide $^{\bullet}O^{2-}$, h^+ photo-induced hole, e^- excited electrons). To investigate their role in the degradation of MB assisted by W-modified TiO_2/SiO_2 catalyst, decomposition experiments were conducted with the addition of KI, IPA, BQ, and DMSO which were reported to be highly reactive to h^+, $^{\bullet}OH$, $^{\bullet}O^{2-}$ and e^-, respectively.[43-45] It is clear that the presence of all four scavengers hinders the decolorization of MB, RhB, MO and CR dyes. DMSO exhibits the highest scavenging performance with 51.63, 43.50, 35.69 and 25.54 %, respectively, drop in decolorization efficiency, while KI only reduces dyes decolorization efficiency by around 12.66 % for MB, 10.62 % for RhB, 9.42 % for MO and 5.14 % for CR. This result shows that the decomposition mainly involves e^- excited electrons and reactivity decreases in the order $e^- \rightarrow {}^{\bullet}O^{2-} \rightarrow {}^{\bullet}OH \rightarrow h^+$ (figure 12).

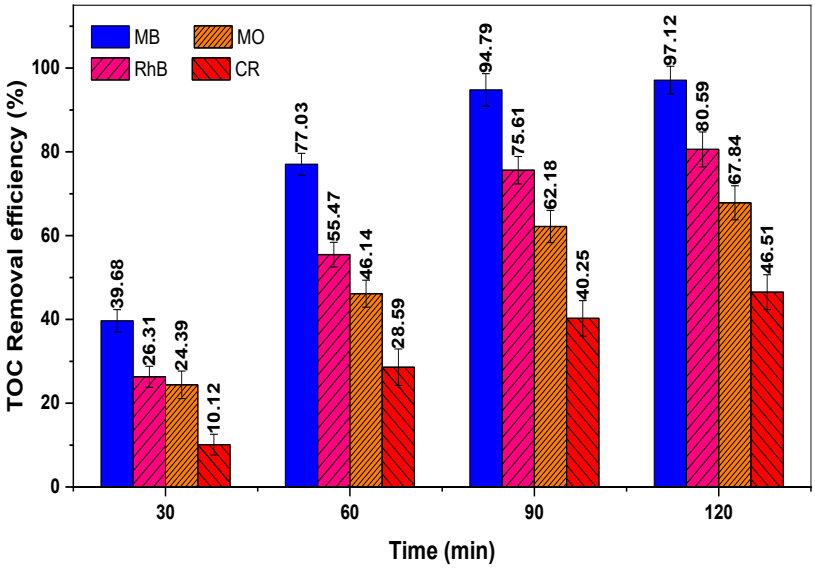

Figure 11: TOC removal efficiency of solutions of MB, RhB, MO and CR dyes in the photocatalytic degradation (V = 500 mL; C_0 = 40 mg.L^{-1}; $m_{catalyst}$ = 300 mg; pH = 9 for MB and RhB and pH = 3 for MO and CR; adsorption time = 60 min. and illumination time from 30 to 120 min.)

The photocatalytic activity of W-modified TiO_2/SiO_2 in the visible light region can be explained by the photocatalytic mechanism of the semiconductors. The absorption edge of the conduction band (E_{CB}) for TiO_2 nanoparticles on SiO_2 was found to be -0.40 eV vs. NHE.[46] The bandgap energy, E_g, based on UV-Vis-DRS analysis of W-modified TiO_2/SiO_2 is 2.85 eV. Therefore, the adsorption edge of the valence band, E_{VB} is considered as $E_{VB} = E_{CB} + E_g$ = -0.40 + 2.85 = 2.45 eV. Under visible light irradiation, the excited electrons (e^-) are transferred to the conduction band (e_{CB}^-) leaving holes (h_{VB}^+) in the valence band (Eq. 5). Because the potential of E_{CB} of TiO_2 loaded SiO_2 (-0.4 eV) is negative than the potential of E_{CB} (+0.4 eV)[47] in WO_3, electrons (e^-) in the conduction band of TiO_2 in W-modified TiO_2/SiO_2 material are easily transferred to W^{6+} ions in WO_3 to form W^{5+} ions (Eq. 6).[16,17] It is known that the potential energy of HOMO and LUMO for MB; RhB; MO and CR are (+1.61 and -0.25 eV);[48] (+1.10 and -1.00 eV);[48] (+0.14 and -1.87 eV)[48] and (-2.24 and -2.73 eV),[41] respectively. Under visible light irradiation, those dyes act as a photosensitive agent that transport their electrons into the conduction band of TiO_2 (Eq. 7-9). The potential of the E_{CB} conduction region of W-TiO_2/SiO_2 (about -0.40 eV) is negative than that of the oxidation potential of $O_2/{}^{\bullet}O^{2-}$ (-0.33 eV)[49,50], so the newly formed W^{5+} ion in Eq. 6 will react directly with O_2 to form superoxide radicals $^{\bullet}O^{2-}$ (Eq. 10).[51] The superoxide radicals continue to react with adsorbed H_2O molecules on the surface of the catalyst

or H^+ ions in the solution to form hydroxyl $^{\bullet}OH$ radicals (Eq. 11-14).[16] Meanwhile, the holes (h_{VB}^+) in the valence band of W-modified TiO_2/SiO_2 react with OH^- at catalyst surface to form $^{\bullet}OH$ radicals (Eq. 15) due to the fact that the potential of (h_{VB}^+) in the valence band of W-TiO_2/SiO_2 (+2.45 eV) is more positive than that of $^{\bullet}OH/OH^-$ (+1.99 eV).[49,50] $^{\bullet}OH$ radicals will, in turn, oxidize dyes adsorbed on the catalyst surface to form degradation products with a decrease in the TOC value of the dye solution (Eq. 16). In addition, holes (h_{VB}^+) in the valence band of W-modified TiO_2/SiO_2 (E = +2.45 eV) can also react directly with MB, RhB, MO and CR dyes (E = +1.61, +1.10, 0.14and -2.24 eV, respectively) (Eq. 17). However, quenching experiments show that the ability to oxidize in this direction is negligible. SiO_2 particles in W-modified TiO_2/SiO_2 composite, with their large specific surface area, assist the accumulation of MB molecules on the catalyst surface, boosting their decomposition on the W-modified TiO_2/SiO_2 surface. The photocatalytic mechanism is proposed as follows[16,17,51]:

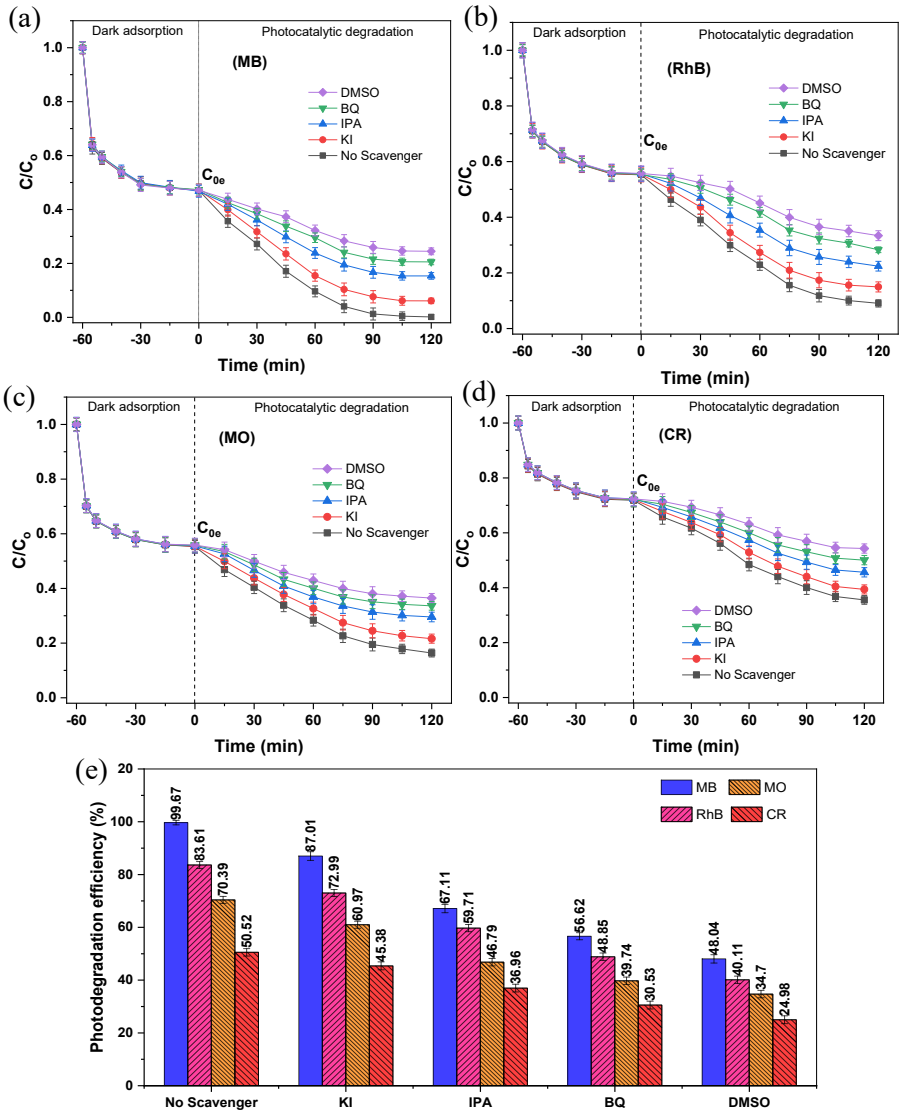

Figure 12: Effect of radical scavengers on decolorization of (a) MB, (b) RhB, (c) MO and (d) CR dyes over W-modified TiO_2/SiO_2 catalyst, and (e) photodegradation efficiency of dyes in case of reaction with the absence and reaction with presence of radical scavengers (V = 500 mL; C_0 = 40 mg.L^{-1}; $m_{catalyst}$ = 300 mg; pH = 9 for MB and RhB and pH = 3 for MO and CR adsorption time = 60 min. and illumination time = 120 min.)

$$W - TiO_2/SiO_2 \xrightarrow{h\nu} W - TiO_2/SiO_2(e_{CB}^-) + W - TiO_2/SiO_2\ (h_{VB}^+) \quad (5)$$

$$W - TiO_2/SiO_2 + W^{6+} \rightarrow W - TiO_2/SiO_2 + W^{5+} \quad (6)$$

$$Dye + h\nu \rightarrow Dye^* \quad (7)$$

$$Dye^* + W - TiO_2/SiO_2 \rightarrow W - \frac{TiO_2}{SiO_2(e_{CB}^-)} + Dye^{*+} \quad (8)$$

$$Dye^{*+} \rightarrow Dye + h_{VB}^+ \quad (9)$$

$W^{5+} + O_2 \rightarrow W^{6+} + {}^{\bullet}O_2^-$ (10)

${}^{\bullet}O_2^- + H_2O \rightarrow {}^{\bullet}HO_2 + OH^-$ (11)

${}^{\bullet}O_2^- + H^+ \rightarrow {}^{\bullet}HO_2$ (12)

$2{}^{\bullet}HO_2 \rightarrow H_2O_2 + O_2$ (13)

$H_2O_2 + W^{6+} \rightarrow W^{5+} + {}^{\bullet}OH + OH^-$ (14)

$W - TiO_2/SiO_2\ (h_{VB}^+) + OH^- \rightarrow W - TiO_2/SiO_2 + {}^{\bullet}OH$ (15)

${}^{\bullet}OH$ + Dye → degradation products (16)

$W - TiO_2/SiO_2(h_{VB}^+)$ (direct holes) + Dye → degradation products (17)

The mechanism is visually illustrated in Figure 13.

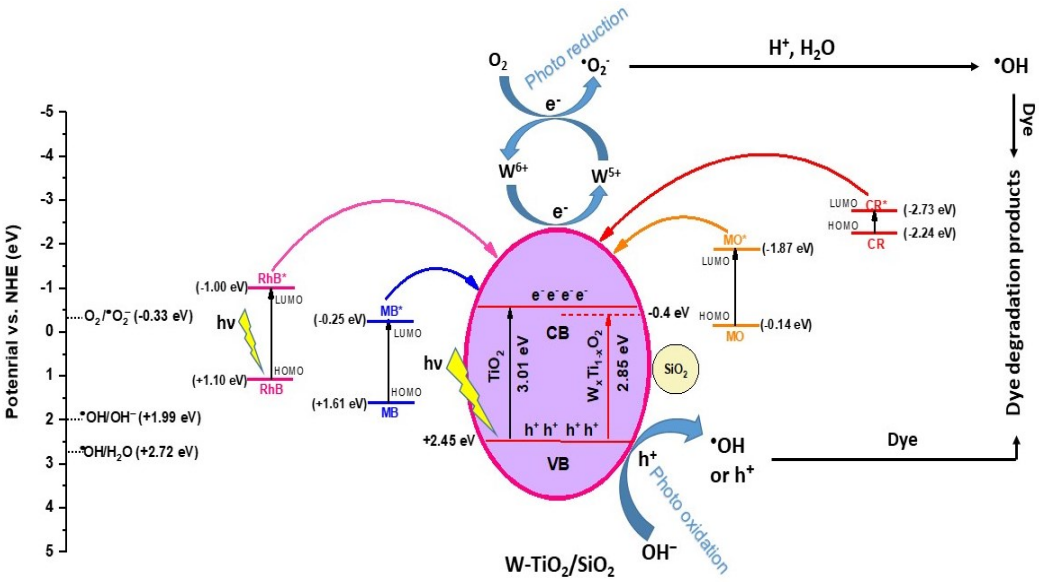

Figure 13: The proposed mechanisms for the photocatalytic degradation of RhB, MB, MO and CR using W-modified TiO_2/SiO_2 catalyst

3.2.4. Kinetics of dyes photocatalytic degradation
Dark adsorption

Figures 14 a-d show the adsorption and photocatalytic kinetics of MB, RhB, MO and CR dyes degradation. The W-modified TiO_2/SiO_2 presents a high adsorption capacity during the dark adsorption period. Depending on the initial dye concentration, the adsorption reaches adsorption/desorption equilibrium around 45-60 minutes.

The equilibrium adsorption capacity, q_e, can be expressed as follows:[52,53]

$$q_e = \frac{V.(C_0 - C_e)}{m} \quad (18)$$

where C_0 and C_e are the dye concentration at initial and equilibrium time (mg.L^{-1}); V is the volume of the dye solution (L); m is the mass of catalyst (g).

The relationship between C_e and q_e is expressed by the Langmuir isotherm model as equation (19) and Freundlich model as equation (20):[52,54]

$$q_e = \frac{K_L.q_m.C_e}{1 + K_L.C_e} \quad (19)$$

$$q_e = K_F.C_e^{1/n} \quad (20)$$

where q_m is the maximum monolayer adsorption capacity (mg.L^{-1}); K_L is the Langmuir adsorption equilibrium constant (L.mg^{-1}); K_F and n are Freundlich parameters.

The non-linear regressions using the equilibrium adsorption data after 60 minutes of MB, RhB, MO and CR dyes dark adsorption over W-modified TiO_2/SiO_2 are shown in table 3. The determination coefficients (0.989 to 0.997) for the Langmuir isotherm model are close to 1 and higher than those (0.945 to 0.958) of the Freundlich isotherm model indicating that the equilibrium data fits well in the Langmuir model.

Kinetics of photocatalytic decomposition

Based on the Langmuir-Hinshelwood model, the overall reaction can be illustrated as follows:

$$W\text{-}TiO_2/SiO_2 + \text{Dye} \underset{k_{-1}}{\overset{k_1}{\rightleftharpoons}} W\text{-}TiO_2/SiO_2\ldots\text{Dye})^* \xrightarrow{k_2} \text{degradation products} \quad (21)$$

where k_1 and k_{-1} are the forward/reversible adsorption rate constant, respectively; k_2 is the rate coefficient of the degradation process.

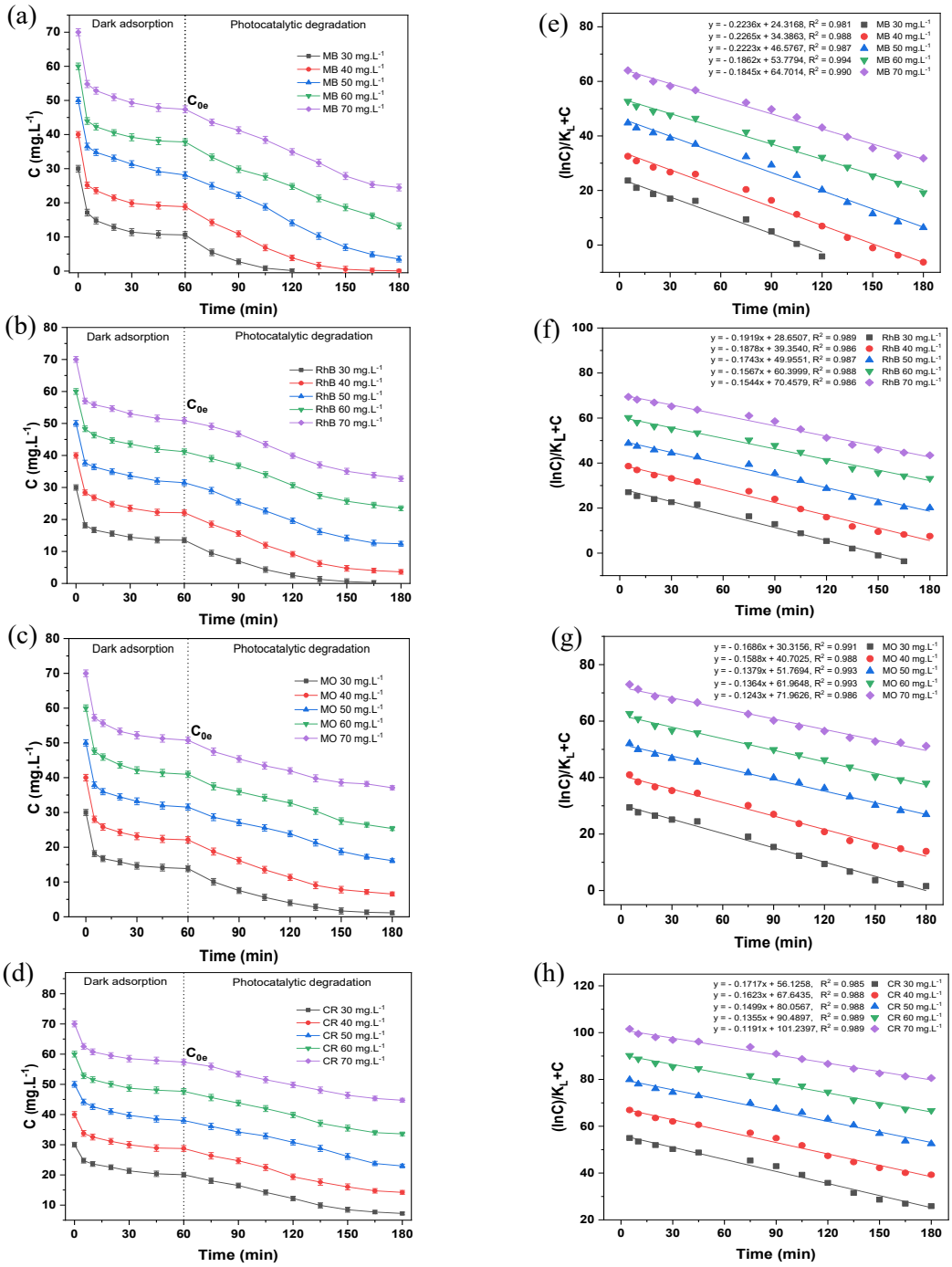

Figure 14: The adsorption and photodegradation kinetics of (a) MB, (b) RhB, (c) MO and (d) CR dyes on W-modified TiO_2/SiO_2 catalyst; The plots of the ($1/K_L$.lnC + C) *vs* time at different initial concentration of (e) MB, (f) RhB, (g) MO and (h) CR dyes

The Langmuir-Hinshelwood model is widely used for unimolecular reaction using heterogeneous catalyst. This equation is described as follows:

$$\ln\frac{C_t}{C_0} = -k_{LH}.t \qquad (22)$$

where C_0 and C_t (mg.L^{-1}) are initial dye concentration and dye concentration at a certain time t (min); k_{LH} (min^{-1}) is a rate constant of the degradation process; The k_{LH} is obtained as the slope of the linear plot of $\ln C_t/C_0$ *vs* t. A kinetic model of the dye decomposition on heterogeneous catalyst based on the Langmuir-Hinshelwood model proposed by Khieu *et al.*[55] in which the combination of equilibrium data in dark adsorption and kinetics data in photocatalytic degradation is taken into account. The equation of this model is described as follows:

$$\frac{1}{K_L}.\ln C + C = -k_{MLH}.t + \frac{1}{K_L}.\ln C_{0e} + C_{0e} \qquad (23)$$

where C_{0e} (mg·L^{-1}) is the equilibrium concentration of adsorbate at time t (min) in which the light is turned on; K_L (L.mg^{-1}) is equilibrium constant given by the Langmuir isotherm model, k_{MLH} is rate constant of photocatalytic reaction.

The plot of the ($1/K_L$.lnC + C) vs t provides a straight line with slope k_{MLH} (figure 14(e)-(h)). In the present study, both models were employed to determine the kinetics data with a comparison. Their parameters are presented in table 4. From table 4, both models exhibit high determination coefficients (R^2 = 0.981 - 0.993), however, in the statistical view of the paired samples t-test, the determination coefficient for the modified Langmuir-Hinshelwood model is significantly higher than those of Langmuir-Hinshelwood one (t (19) = 5.4, $p \leq 0.001 < \alpha = 0.05$). It means that experimental data is more compatible with the modified Langmuir-Hinshelwood model than the Langmuir-Hinshelwood one. At the initial 30 mg.L^{-1} MB, RhB, MO and CR dyes, the first order rate constants, k_{LH} obtained were the largest (7.99×10^{-2}, 3.98×10^{-2}, 2.24×10^{-2} and 0.95×10^{-2} min^{-1}) and they tend to decrease with increasing dye concentration from 30-70 mg.L^{-1} indicating that W-modified TiO_2/SiO_2 material is suitable for degradation of dyes at relatively low concentrations. Table 5 lists the rate constant (k_{LH}) of dyes photocatalytic decomposition on various catalysts reported previously. It is obvious that the rate constant in the present work is comparable or even higher than those in previous works indicating that the W-modified TiO_2/SiO_2 exhibits faster kinetics.

Table 3: The parameters of Langmuir and Freundlich models

Dyes	Langmuir isotherm model			Freudlich isotherm model		
	K_L (L.mg^{-1})	q_m (mg.g^{-1})	R^2	K_F	n	R^2
MB	0.436	39.39	0.997	26.07	10.27	0.958
RhB	0.326	33.81	0.996	21.07	9.30	0.952
MO	0.257	34.67	0.991	19.50	7.68	0.945
CR	0.106	24.67	0.989	8.90	4.62	0.951

Table 4: The value of k_{MLH} and k_{LH} at different initial concentrations of MB, RhB, MO and CR dyes over W-modified TiO_2/SiO_2 catalyst

Dyes	C_o (mg.L^{-1})	Modified Langmuir-Hinshelwood		Langmuir-Hinshelwood	
		k_{MLH} ($\times10^{-2}$ mg·L^{-1}·min^{-1})	R^2	k_{LH} ($\times10^{-2}$ min^{-1})	R^2
MB	30	22.36	0.981	7.99	0.966
	40	22.65	0.988	5.33	0.962
	50	22.23	0.987	1.96	0.977
	60	18.62	0.994	0.86	0.984
	70	18.45	0.990	0.60	0.987
RhB	30	19.19	0.989	3.98	0.981
	40	18.78	0.986	1.70	0.983
	50	17.43	0.987	0.88	0.983
	60	15.67	0.988	0.52	0.982
	70	15.44	0.986	0.41	0.980
MO	30	16.86	0.991	2.24	0.989
	40	15.88	0.988	1.06	0.984
	50	13.79	0.993	0.58	0.985
	60	13.64	0.993	0.40	0.986
	70	12.43	0.986	0.24	0.977
CR	30	17.17	0.985	0.95	0.985
	40	16.23	0.988	0.64	0.985
	50	14.99	0.988	0.46	0.984
	60	13.55	0.989	0.32	0.985
	70	11.91	0.989	0.22	0.984

Table 5: Comparison of rate constant of the present catalyst with published literature

Catalyst	Dye	Light source	C_0 (mg/L)/ Volume (mL) /$m_{catalyst}$ (mg)	$K = k_{LH}/m_{catalyst}$ ($min^{-1}.g^{-1}$)	Ref.
W-modified TiO_2/SiO_2	MB	45W Compact lamp (λ > 420 nm)	30/500/300	**0.2663**	The present work
TiO_2	MB	125W Philips lamp	26.9/2750/375	0.0667	[56]
W-loaded TiO_2	MB	250W metal halide lamp	40/100/1000	0.0280	[54]
Fe_3O_4/ZnO/BiOI/PANI	MB	LED lamp (50 W)	3.2/250/100	0.1810	[57]
TiO_2@SiO_2-Ag	MB	Sunlight irradiation	10/100/100	0.2996	[58]
$CuInS_2$ nanoparticles	MB	LED light (λ > 400 nm)	10/200/100	0.0059	[59]
W-modified TiO_2/SiO_2	RhB	45W Compact lamp (λ > 420 nm)	30/500/300	**0.1327**	The present work
C and N Co-doped TiO_2	RhB	36W compact lamp	30/100/180	0.0817	[60]
Fe_3O_4/ZnO/PANI	RhB	LED lamp (50 W)	4.79/250/100	0.0225	[57]
Fe_3O_4/ZnO/BiOI/PANI	RhB	LED lamp (50 W)	4.79/250/100	0.2260	[57]
$CuInS_2$ nanoparticles	RhB	LED light (λ > 400 nm)	10/200/100	0.1240	[59]
C-doped ZnO	RhB	350W Xenon lamp	1/100/100	0.1570	[44]
W-modified TiO_2/SiO_2	MO	45W Compact lamp (λ > 420 nm)	30/500/300	**0.0747**	The present work
Degussa P25 TiO_2	MO	Natural solar radiation	8.18/200/1500	0.0420	[61]
Fe_3O_4/ZnO/BiOI/PANI	MO	LED lamp (50 W)	3.27/250/100	0.0207	[57]
W-loaded TiO_2	MO	250W metal halide lamp	40/100/1000	0.0034	[54]
Cu-doped TiO_2	MO	365 nm UV lamp	15/1000/2000	0.0080	[62]
Co:La:TiO_2 nanocomposite	MO	visible ligh	100/1000/800	0.0533	[63]
W-modified TiO_2/SiO_2	CR	45W Compact lamp (λ > 420 nm)	30/500/300	**0.0317**	The present work
TiO_2 Degussa (P-25)	CR	mercury UV lamp + O_2	55/1000/1000	0.0047	[64]
WO_3–TiO_2/AC	CR	500W mercury-vapour lamp	30/2000/10000	0.0028	[65]
g-C_3N_4/CdS	CR	100 W halogen lamp	20/250/100	0.0406	[66]
ZnO/rGO	CR	UV lamp	10/1000/2000	0.0459	[67]
Na-ZnO	CR	Sunlight irradiation	32/50/500	0.0600	[68]

3.2.5. Recyclability

Recycling of catalysts is one of the critical criteria to develop heterogeneous photocatalytic technology for wastewater treatment. Hence, the recyclability of W-modified TiO_2/SiO_2 for adsorption and the photocatalytic process was performed. The used catalysts were separated, washed by ethanol for several times and dried for 24 h at 100 ºC before being reused.

The reused catalyst was utilized to degrade MB repeatedly (figure 15a). W-modified TiO_2/SiO_2 presented a slight loss of catalytic activity after 3 cycles with the efficiency reducing from 99.51% to 92.14%. XRD patterns of original and reused catalysts stay unchanged (figure 15b) indicating that the catalysts are stable during the adsorption and photocatalytic process.

4. CONCLUSIONS

The synthesis of W-modified TiO_2/SiO_2 composites and its application for photocatalytic decomposition of MB, RhB, MO and CR dyes in visible light were investigated. The morphology of W-modified TiO_2/SiO_2 consists of 3-5-nanometer W-modified TiO_2 nanoparticles highly dispersed on the silica matrix. W-modified TiO_2/SiO_2 possesses a large specific surface area and enhances the visible light absorption. The photocatalytic decomposition of MB, RhB, MO and CR dyes on W-modified TiO_2/SiO_2 is about 9 times higher than that of TiO_2 under visible light. The enhanced photocatalytic activity is attributed to the capability of W-doping to narrow the bandgap energy and prolong the recombination of photoinduced electron/hole pairs. Kinetic data of dyes decomposition is well fitted to the modified Langmuir-Hinshelwood model based on a combination of the Langmuir isotherms and first-order kinetic equations. The W-modified TiO_2/SiO_2 material is stable for recycling and can be used effectively for the photocatalytic decomposition for both different types of dyes - cations and anions, offering a potential photocatalyst for treating dyes in

aqueous solutions.

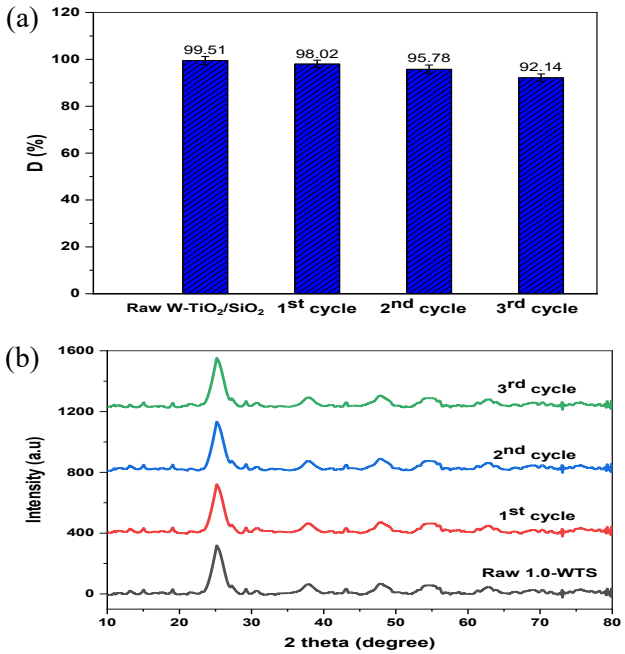

Figure 15: (a) Photocatalytic degradation efficiency of used catalysts; (b) XRD patterns of W - modified TiO_2/SiO_2 after three photocatalytic testing cycles (V = 500 mL, C_0 = 40 mg.L^{-1}, $m_{catalyst}$ = 300 mg; adsorption time is 60 min.; light-illumination time is 120 min.)

REFERENCES

1. H. J. Perera. Removal of acid orange 7 dye from wastewater: Review, *Int. J. Waste Resour.*, **2019**, *9(1)*, 1-4.
2. Y.-H. Chiu, T.-F.M. Chang, C.-Y. Chen, M. Sone, Y.-J. Hsu. Mechanistic insights into photodegradation of organic dyes using heterostructure photocatalysts, *Catalysts*, **2019**, *9(5)*, 430.
3. Z.-H. Zhang, J.-L. Zhang, J.-H. Liu, Z.-H. Xiong, X. Chen. Selective and competitive adsorption of azo dyes on the metal-organic framework ZIF-67, *Water Air Soil Pollut*, **2016**, *227(12)*, 471.
4. B. Shi, G. Li, D. Wang, C. Feng, H. Tang. Removal of direct dyes by coagulation: the performance of preformed polymeric aluminum species, *J. Hazard Mater.*, **2007**, *143(1-2)*, 567-574.
5. A. M. Faouzi, B. Nasr, G. Abdellatif. Electrochemical degradation of anthraquinone dye alizarin red S by anodic oxidation on boron-doped diamond, *Dyes Pigm*, **2007**, *73(1)*, 86-89.
6. D. Ayodhya, G. Veerabhadram. A review on recent advances in photodegradation of dyes using doped and heterojunction based semiconductor metal sulfide nanostructures for environmental protection, *Mater. Today Eng*, **2018**, *9*, 83-113.
7. H. Tian, J. Ma, K. Li, J. Li. Photocatalytic degradation of methyl orange with W-doped TiO_2 synthesized by a hydrothermal method, *Mater. Chem. Phys.*, **2008**, *112(1)*, 47-51.
8. A. Mills, R.H. Davies, D. Worsley. Water purification by semiconductor photocatalysis, *Chem. Soc Rev.*, **1993**, *22*, 417-425.
9. L. Xu, C.-Q. Tang, J. Qian, Z.-B. Huang. Theoretical and experimental study on the electronic structure and optical absorption properties of P-doped TiO_2, *Appl Surf Sci*, **2010**, *256(9)*, 2668-2671.
10. Y. Bessekhouad, D. Robert, J.V. Weber, N. Chaoui. Effect of alkaline-doped TiO_2 on photocatalytic efficiency, *J. Photochem. Photobiol A: Chem*, **2004**, *167(1)*, 49-57.
11. N. Venkatachalam, M. Palanichamy, B. Arabindoo, V. Murugesan. Alkaline earth metal doped nanoporous TiO_2 for enhanced photocatalytic mineralisation of bisphenol-A, *Catal Commun*, **2007**, *8(7)*, 1088-1093.
12. W. Choi, A. Termin, M. R. Hoffmann. The role of metal ion dopants in duantum-sized TiO_2: Correlation between photoreactivity and charge carrier recombination dynamics, *J. Phys. Chem. C*, **1994**, *98*, 13669-13679.
13. L. G. Devi, B. N. Murthy, S. G. Kumar. Photocatalytic activity of TiO_2 doped with Zn^{2+} and V^{5+} transition metal ions: Influence of crystallite size and dopant electronic configuration on photocatalytic activity, *Mater Sci Eng: B*, **2010**, *166(1)*, 1-6.
14. J. Xu, Y. Ao, D. Fu, C. Yuan. A simple route to synthesize highly crystalline N-doped TiO_2 particles under low temperature, *J. Cryst. Growth*, **2008**, *310(19)*, 4319-4324.
15. X. Z. Li, L. F. B., Y. C. L., W. K. Ge. Photocatalytic activity of WO_x-TiO_2 under visible light irradiation, *J Photochem Photobiol A: Chem*, **2001**, *141(2-3)*, 209-217.
16. O. Avilés-García, J. Espino-Valencia, R. Romero, J.L. Rico-Cerda, M. Arroyo-Albiter, R. Natividad. W and Mo doped TiO_2: Synthesis, characterization and photocatalytic activity, *Fuel*, **2017**, *198*, 31-41.
17. M. Jin, X. Zhang, H. Pu, S. Nishimoto, T. Murakami, A. Fujishima. Photochromism-based detection of volatile organic compounds by W-doped TiO_2 nanofibers, *J. Collo. Inter. Sci.*, **2011**, *362(1)*, 188-193.
18. B. Xing, C. Shi, C. Zhang, G. Yi, L. Chen, H. Guo, G. Huang, J. Cao. Preparation of TiO_2/Activated carbon composites for photocatalytic degradation of RhB under UV light irradiation, *J Nanomater*, **2016**, *2016*, 1-10.

19. Y. Liu, H. Yu, Z. Lv, S. Zhan, J. Yang, X. Peng, Y. Ren, X. Wu. Simulated-sunlight-activated photocatalysis of methylene blue using cerium-doped SiO_2/TiO_2 nanostructured fibers, *J. Environ. Sci.*, **2012**, *24(10)*, 1867-1875.
20. R. -L. Dong, C. Na, H. -P. Zhang, Z. -D. Chen, C. -C. Jin. TiO_2/SiO_2 mesoporous microspheres with intelligently controlled texture, *Mater. Des.*, **2016**, *89*, 830-838.
21. G. N. Shao, Y. Kim, S. M. Imran, S. J. Jeon, P. B. Sarawade, A. Hilonga, J. -K. Kim, H. T. Kim. Enhancement of porosity of sodium silicate and titanium oxychloride based TiO_2-SiO_2 systems synthesized by sol-gel process and their photocatalytic activity, *Micropor. Mesopor. Mater.*, **2013**, *179*, 111-121.
22. Z. Huang, P. Wu, B. Gong, X. Zhang, Z. Liao, P. -C. Chiang, X. Hu, L. Cui. Immobilization of visible light-sensitive (N, Cu) co-doped TiO_2 onto rectorite for photocatalytic degradation of p-chlorophenol in aqueous solution, *Appl. Clay Sci.*, **2017**, *142*, 128-135.
23. M. Valera-Zaragoza, A. Yescas-Yescas, E. A. Juarez-Arellano, A. Aguirre-Cruz, A. Aparicio-Saguilán, E. Ramírez-Vargas, S. Sepúlveda-Guzmán, S. Sánchez-Valdes. Immobilization of TiO_2 nanoparticles on montmorillonite clay and its effect on the morphology of natural rubber nanocomposites, *Poly. Bull*, **2014**, *71(6)*, 1295-1313.
24. C. Ren, W. Qiu, Y. Chen. Physicochemical properties and photocatalytic activity of the TiO_2/SiO_2 prepared by precipitation method, *Sep. Purif Technol.*, **2013**, *107*, 264-272.
25. C. Chen, X. Liu, H. Long, F. Ding, Q. Liu, X. A. Chen. Preparation and photocatalytic performance of graphene Oxide/WO_3 quantum Dots/TiO_2@SiO_2 microspheres, *Vacuum*, **2019**, *164*, 66-71.
26. H. Chen, X. Wang, J. Li, X. Wang. Cotton derived carbonaceous aerogels for the efficient removal of organic pollutants and heavy metal ions, *J. Mater. Chem A*, **2015**, *3(11)*, 6073-6081.
27. F. Chen, E. Zhao, T. Kim, J. Wang, G. Hableel, P. J. T. Reardon, S. J. Ananthakrishna, T. Wang, S. Arconada-Alvarez, J. C. Knowles, J.V. Jokerst. Organosilica nnoparticles with an intrinsic secondary amine: An efficient and reusable adsorbent for dyes, *ACS Appl. Mater. Interfaces,* **2017**, *9(18)*, 15566-15576.
28. E. Lorenc-Grabowska, P. Rutkowski. Tailoring mesoporosity of poly(furfuryl alcohol)-based activated carbons and their ability to adsorb organic compounds from water, *J. Mater. Cycles Waste Manag.*, **2018**, *20(3)*, 1638-1647.
29. A. Jaroenworaluck, N. Pijarn, N. Kosachan, R. Stevens. Nanocomposite TiO_2-SiO_2 gel for UV absorption, *Chem. Eng. J.*, **2012**, 181-182, 45-55.
30. M. Mohammadi, M. Sedighi, V. Alimohammadi. Modeling and optimization of nitrate and total iron removal from wastewater by TiO_2/SiO_2 nanocomposites, *Int. J. Nano Dimens*, **2019**, *10(2)*, 195-208.
31. C. Hao, J. Li, Z. Zhang, Y. Ji, H. Zhan, F. Xiao, D. Wang, B. Liu, F. Su. Enhancement of photocatalytic properties of TiO_2 nanoparticles doped with CeO_2 and supported on SiO_2 for phenol degradation, *Appl. Surf. Sci.*, **2015**, *331*, 17-26.
32. M. Samadi, H.A. Shivaee, M. Zanetti, A. Pourjavadi, A. Moshfegh. Visible light photocatalytic activity of novel MWCNT-doped ZnO electrospun nanofibers, *J. Mol Catal. A: Chem*, **2012**, *359*, 42-48.
33. S. Dagher, A. Soliman, A. Ziout, N. Tit, A. Hilal-Alnaqbi, S. Khashan, F. Alnaimat, J.A. Qudeiri. Photocatalytic removal of methylene blue using titania- and silica-coated magnetic nanoparticles, *Mater. Res. Express*, **2018**, *5(6)*, 065518.
34. Y. Chimupala, G. Hyett, R. Simpson, R. Mitchell, R. Douthwaite, S.J. Milne, R.D. Brydson. Synthesis and characterization of mixed phase anatase TiO_2 and sodium-doped TiO_2(B) thin films by low pressure chemical vapour deposition (LPCVD), *RSC Adv.*, **2014**, *4(89)*, 48507-48515.
35. W. Chang, L. Yan, L. Bin, R. Sun. Photocatalyic activity of double pore structure TiO_2/SiO_2 monoliths, *Ceram Int.*, **2017**, *43(8)*, 5881-5886.
36. Z. Fang, T. Lin, H. Xu, G. Wu, M. Sun, Y. Chen. Novel promoting effects of cerium on the activities of NO_x reduction by NH_3 over TiO_2-SiO_2-WO_3 monolith catalysts, *J. Rare Earths*, **2014**, *32(10)*, 952-959.
37. H. Wan, W. Yao, W. Zhu, Y. Tang, H. Ge, X. Shi, T. Duan. Fe-N co-doped SiO_2@TiO_2 yolk-shell hollow nanospheres with enhanced visible light photocatalytic degradation, *Appl. Surf. Sci.*, **2018**, *444*, 355-363.
38. C. Ren, W. Qiu, H. Zhang, Z. He, Y. Chen. Degradation of benzene on $TiO_2/SiO_2/Bi_2O_3$ photocatalysts under UV and visible light, *J. Mol Catal A: Chem.*, **2015**, *398*, 215-222.
39. A. Baral, D.P. Das, M. Minakshi, M.K. Ghosh, D.K. Padhi. Probing environmental remediation of RhB organic dye using α-MnO_2 under visible- light irradiation: Structural, photocatalytic and mineralization studies, *Chemistry Select*, **2016**, *1(14)*, 4277-4285.
40. H. Dong, C. Sans, W. Li, Z. Qiang. Promoted discoloration of methyl orange in H_2O_2/Fe(III) Fenton system: Effects of gallic acid on iron cycling, *Sep Purif Technol.*, **2016**, *171*, 144-150.
41. C. Chimeno-Trinchet, A. Fernandez-Gonzalez, J.A. Garcia Calzon, M. E. Diaz-Garcia, R. Badia Laino. Alkyl-capped copper oxide nanospheres and

nanoprolates for sustainability: Water treatment and improved lubricating performance, *Sci. Technol. Adv. Mater.*, **2019**, *20(1)*, 657-672.

42. Z. Cao, T. Zhang, P. Ren, D. Cao, Y. Lin, L. Wang, B. Zhang, X. Xiang. Doping of chlorine from a neoprene adhesive enhances degradation efficiency of dyes by structured TiO_2-coated photocatalytic fabrics, *Catalysts*, **2020**, *10(1)*, 69.
43. A. Abdessemed, S. Rasalingam, S. Abdessemed, K. E. Z. Djebbar, R. Koodali. Impregnation of ZnO onto a vegetal activated carbon from algerian olive waste: A sustainable photocatalyst for degradation of ethyl violet dye, *Int. J. Photoenergy*, **2019**, *2019*, 1-13.
44. Y. Zhang, J. Zhou, X. Chen, Q. Feng, W. Cai. MOF-derived C-doped ZnO composites for enhanced photocatalytic performance under visible light, *J. Alloy Comp.*, **2019**, *777*, 109-118.
45. 45. W. Wang, K. Xiao, L. Zhu, Y. Yin, Z. Wang. Graphene oxide supported titanium dioxide & ferroferric oxide hybrid, a magnetically separable photocatalyst with enhanced photocatalytic activity for tetracycline hydrochloride degradation, *RSC Adv.*, **2017**, *7(34)*, 21287-21297.
46. 46. M. Perego, G. Seguini, G. Scarel, M. Fanciulli, F. Wallrapp. Energy band alignment at TiO_2/Si interface with various interlayers, *J. Appl. Phys.*, **2008**, *103(4)*, 043509.
47. X. Zeng, Z. Wang, G. Wang, T. R. Gengenbach, D. T. McCarthy, A. Deletic, J. Yu, X. Zhang. Highly dispersed TiO_2 nanocrystals and WO_3 nanorods on reduced graphene oxide: Z-scheme photocatalysis system for accelerated photocatalytic water disinfection, *Appl. Catal B: Environ*, **2017**, *218*, 163-173.
48. Q. Li, X. Li, S. Wageh, A. A. Al-Ghamdi, J. Yu. CdS/Graphene nanocomposite photocatalysts, *Adv. Energy Mater.*, **2015**, *5(14)*, 1500010.
49. B. Lin, C. Xue, X. Yan, G. Yang, G. Yang, B. Yang. Facile fabrication of novel SiO_2/g-C_3N_4 core-shell nanosphere photocatalysts with enhanced visible light activity, *Appl. Surf Sci.*, **2015**, *357*, 346-355.
50. W. Wang, J. C. Yu, D. Xia, P. K. Wong, Y. Li. Graphene and g-C_3N_4 nanosheets cowrapped elemental alpha-sulfur as a novel metal-free heterojunction photocatalyst for bacterial inactivation under visible-light, *Environ. Sci. Technol.*, **2013**, *47(15)*, 8724-8732.
51. B. Tatykayev, F. Donat, H. Alem, L. Balan, G. Medjahdi, B. Uralbekov, R. Schneider. Synthesis of core/shell ZnO/rGO nanoparticles by calcination of ZIF-8/rGO composites and their photocatalytic activity, *ACS Omega*, **2017**, *2(8)*, 4946-4954.
52. Saepurahman M. A., Abdullah, F. K. Chong. Dual-effects of adsorption and photodegradation of methylene blue by tungsten-loaded titanium dioxide, *Chem. Eng. J.*, **2010**, *158(3)*, 418-425.
53. F. Motahari, M. R. Mozdianfard, F. Soofivand, M. Salavati-Niasari. NiO nanostructures: Synthesis, characterization and photocatalyst application in dye wastewater treatment, *RSC Adv.*, **2014**, *4(53)*, 27654-27660.
54. Saepurahman, M. A. Abdullah, F. K. Chong. Preparation and characterization of tungsten-loaded titanium dioxide photocatalyst for enhanced dye degradation, *J. Hazard Mater.*, **2010**, *176(1-3)*, 451-458.
55. T. T. Minh, N. T. T. Tu, T. T. Van Thi, L. T. Hoa, H. T. Long, N. H. Phong, T. L. M. Pham, D. Q. Khieu. Synthesis of porous octahedral ZnO/CuO composites from Zn/Cu-based MOF-199 and their applications in visible-light-driven photocatalytic degradation of dyes, *J. Nanomater.*, **2019**, *2019*, 1-16.
56. A. Houas, H. Lachheb, M. Ksibi, E. Elaloui, C. Guillard, J. -M. Herrmann. Photocatalytic degradation pathway of methylene blue in water, *Appl. Catal. B: Environ*, **2001**, *31(2)*, 145-157.
57. A. Habibi-Yangjeh, M. Shekofteh-Gohari. Synthesis of magnetically recoverable visible-light-induced photocatalysts by combination of Fe_3O_4/ZnO with BiOI and polyaniline, *Prog. Nat. Sci.: Mater. Int.*, **2019**, *29(2)*, 145-155.
58. P. Govindhan, C. Pragathiswaran. Synthesis and characterization of TiO_2@SiO_2-Ag nanocomposites towards photocatalytic degradation of rhodamine B and methylene blue, *J Mater Sci: Mater Electron*, **2016**, *27(8)*, 8778-8785.
59. N. Chumha, W. Pudkon, A. Chachvalvutikul, T. Luangwanta, C. Randorn, B. Inceesungvorn, A. Ngamjarurojana, S. Kaowphong. Photocatalytic activity of $CuInS_2$ nanoparticles synthesized via a simple and rapid microwave heating process, *Mater. Res. Express*, **2020**, *7(1)*.
60. T. T. T. Le, T. D. Tran. Photocatalytic degradation of rhodamine B by C and N codoped TiO_2 nanoparticles under visible-light irradiation, *J. Chem.*, **2020**, *2020*, 1-8.
61. D. Ljubas, G. Smoljanic, H. Juretic. Degradation of methyl orange and congo red dyes by using TiO_2 nanoparticles activated by the solar and the solar-like radiation, *J. Environ Manag.*, **2015**, *161*, 83-91.
62. T. Nguyen Thi Thu, N. Nguyen Thi, V. Tran Quang, K. Nguyen Hong, T. Nguyen Minh, N. Le Thi Hoai. Synthesis, characterisation, and effect of pH on degradation of dyes of copper-doped TiO_2, *J. Experimental Nanosci.*, **2015**, *11(3)*, 226-238.
63. K. Azad, P. Gajanan. Photodegradation of methyl orange in aqueous solution by the visible light active Co:La:TiO_2 nanocomposite, *Chem. Sci. J.*, **2017**, *8(3)*,

1000164.

64. L. Ćurković, D. Ljubas, H. Juretić. Photocatalytic decolorization kinetics of diazo dye congo red aqueous solution by UV/TiO_2 nanoparticles, *React. Kinet. Mech. Catal.*, **2009**, *99(1)*, 201-208.
65. J. -H. Sun, Y. -K. Wang, R. -X. Sun, S. -Y. Dong. Photodegradation of azo dye Congo Red from aqueous solution by the WO_3-TiO_2/activated carbon (AC) photocatalyst under the UV irradiation, *Mater. Chem. Phys.*, **2009**, *115(1)*, 303-308.
66. R. C. Pawar, V. Khare, C. S. Lee. Hybrid photocatalysts using graphitic carbon nitride/cadmium sulfide/reduced graphene oxide (g-C_3N_4/CdS/RGO) for superior photodegradation of organic pollutants under UV and visible light, *Dalton Trans.*, **2014**, *43(33)*, 12514-12527.
67. Y. L. Pang, S. F. Tee, S. Lim, A. Z. Abdullah, H. C. Ong, C. -H. Wu, W. C. Chong, A. W. Mohammadu, E. Mahmoudi. Enhancement of photocatalytic degradation of organic dyes using ZnO decorated on reduced graphene oxide (rGO), *Desalin. Water. Treat.*, **2018**, *108*, 311-321.
68. T. M. Elmorsi, M .H. Elsayed, M. F. Bakr. Na doped ZnO nanoparticles assisted photocatalytic degradation of congo red dye using solar light, *Am. J. Chem.*, **2017**, *7(2)*, 48-57.

Corresponding author: **Dinh Quang Khieu**
University of Sciences, Hue University
77 Nguyen Hue, Phu Nhuan, Hue City, Thua Thien Hue 53000, Viet Nam
E-mail: dqkhieu@hueuni.edu.vn.